Magnetic Nozzle Design for High-Power MPD Thrusters

IEPC-2005-230

Presented at the 29th International Electric Propulsion Conference, Princeton University, October 31 – November 4, 2005

Robert P. Hoyt*
Tethers Unlimited, Inc., Bothell, WA, 98011, USA

Abstract: Magnetoplasmadynamic (MPD) thrusters can provide the high-specific impulse, high-power propulsion required to enable ambitious Human and Robotic Exploration missions to the Moon, Mars, and outer planets. MPD thrusters, however, have traditionally been plagued by poor thrust efficiencies. In most operating modes, these inefficiencies are caused primarily by deposition of power into the anode due to the anode fall voltage. Prior investigations have indicated that the Hall Effect term in Ohm's law causes depletion of the plasma near the anode surface, which in turn results in the anode fall and onset behavior contributing to rapid electrode erosion. Under a NASA/GRC Phase I SBIR Phase I effort, we have used analytical methods and the MACH2 code to first investigate the impacts of the Hall term on the behavior of MPD thrusters and then to evaluate several magnetic nozzle concepts for their ability to counter the Hall-induced starvation effects. Through a process of iteration between custom magnetic field design tools and the plasma simulations, developed new magnetic nozzle designs for both the GRC Benchmark MPD thruster. We then designed and fabricated a prototype suitable for testing on the GRC Benchmark thruster in a vacuum chamber facility. If these magnetic nozzles prove successful in minimizing anode fall losses, they could result in dramatic improvements in the thrust efficiency of MPD devices.

I. Nomenclature

$\boldsymbol{B}$	=	magnetic field vector
e	=	electron charge
$\boldsymbol{E}$	=	electric field vector
f	=	distribution function
J_{crit}	=	critical current density
$J_{e,th}$	=	electron thermal current
$\boldsymbol{J}$	=	current density vector
m_e	=	electron mass
n_e	=	electron density
P	=	electron pressure
$q_{e,i}$	=	electron and ion charges
$T_{e,i}$	=	electron and ion temperatures
v	=	velocity
V_A	=	anode bias voltage
$\boldsymbol{V}$	=	voltage vector
σ	=	plasma conductivity
Ω	=	electron Hall parameter

* President, CEO, & Chief Scientist, hoyt@tethers.com

II. Introduction

Magnetoplasmadynamic (MPD) thrusters, also known as Lorentz Force Accelerators (LFA), can provide the high-specific impulse, high-power propulsion required to enable ambitious Human and Robotic Exploration missions to the Moon, Mars, and outer planets. MPD thrusters, however, have traditionally been plagued by poor thrust efficiencies. In most operating modes, these inefficiencies are due primarily to power deposited into the anode due to acceleration of the electron current into the anode surface by a voltage drop, called the "anode fall voltage", which develops in the region near the anode surface.[1,2] Prior investigations have indicated that the Hall Effect term in Ohm's law causes depletion of the plasma near the anode surface.[3] This depletion in turn results in the anode fall and current and voltage oscillations called "onset" behavior, which are associated with rapid electrode erosion.

As part of a NASA/GRC Phase I SBIR effort, we have investigated the use of applied magnetic fields to counter the Hall Effect in the anode region. Using detailed numerical simulations, we first evaluated the impact of the Hall Effect upon the current and plasma density profiles in MPD thrusters, and showed that this term causes concentration of the current onto a small portion of the anode surface and depletion of the anode surface plasma in this region, both of which effects will contribute to the anode fall and anode erosion. Using custom magnetic field design tools, we developed novel magnetic field topologies that provide strong fields intersecting the anode surface. We then used numerical plasma simulation tools to demonstrate that these applied fields can maintain high plasma density in the anode region and achieve smooth distribution of current density along the thruster acceleration channel, both of which will serve to reduce or eliminate the anode fall and mitigate anode erosion. With proper design, the magnetic nozzles also can help to focus the plasma plume in the axial direction while minimizing momentum losses due to detachment of the plasma from the field, maximizing the net thrust extracted from the plasma. Simulations of the GRC Benchmark thruster with and without the optimized magnetic nozzles indicate that thrust efficiencies can be improved by 50% at low power levels and by even larger factors at high power levels. Based upon the results of the simulations, we have developed and constructed a prototype of a magnetic nozzle optimized for the GRC Benchmark thruster geometry

III. Background

A. MPD Thrusters

Magnetoplasmadynamic (MPD) thrusters are relatively simple, compact, and mechanically robust devices that can provide high specific impulse propulsion with high thrust densities. An idealized schematic of an MPD thruster with a simple coaxial geometry is shown in Figure 1. An MPD thruster consists of two concentric electrodes. A propellant gas is fed into the annular region between the electrodes, and a voltage is applied between the electrodes. The applied voltage causes an electrical breakdown in the gas, ionizing it to create a conducting plasma. The applied voltage drives a radial current **J** between the electrodes, carried by the plasma, and this current induces an azimuthal "self" magnetic field **B** in the thruster. The radial current flowing across this azimuthal field causes a Lorentz **J**x**B** force on the plasma in the direction perpendicular to both the current and magnetic field. The Lorentz force accelerates the plasma out of the thruster in the axial direction, producing a high velocity exhaust. Because they use the Lorentz force to accelerate the plasma, MPD thrusters are sometimes referred to as "Lorentz Force Accelerators" (LFA). In plasma fusion research, similar devices are often referred to as "Coaxial Plasma Accelerators". Because they use electromagnetic forces to accelerate the plasma rather than chemical reactions, MPD thrusters can achieve much higher exhaust velocities than chemical rockets, and thus can achieve very high specific impulses. MPD thruster Isp's can range from on the order of 1500 s to over 10,000 s, depending upon the current, mass flow rate, and propellant gas used.

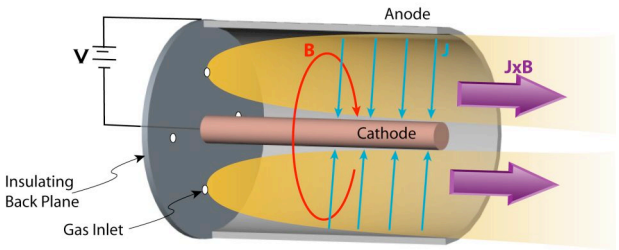

Figure 1. Schematic of a MPD thruster with a simple coaxial geometry.

The recent re-focusing of NASA's efforts upon the Vision for Space Exploration has increased the importance of systems able to support ambitious manned and robotic missions to Mars and the Moon. These developments have renewed interest in developing electric propulsion systems capable of processing large amounts of power; human

exploration mission concepts using electric propulsion typically call for propulsion systems operating from 100 kW up to megawatts of power. Over the past decade, ion and Hall thruster technologies have received the majority of attention and funding due to their technical maturity and excellent efficiency. However, due to space charge limitations, ion and Hall thrusters are not able to readily scale up to very large power levels, and thus they are limited to relatively low thrust densities. An ion-thruster based propulsion system operating at megawatts of power would require many large ion thruster devices, with a total area of tens or hundreds of square meters, to process that amount of power. MPD thrusters, on the other hand, have received very little serious consideration in recent years, primarily due to their traditionally poor thrust efficiencies. Their capability for high thrust density operation has recently resulted in renewed interest and funding for their development. Moreover, because they can be operated both in pulsed and continuous modes, MPD thrusters can readily scale from very low power levels to very high power levels.

B. MPD Thruster Efficiency

The Achilles Heel of MPD thrusters, and the primary reason NASA and commercial enterprises have passed them over in favor of Hall thrusters, is that they typically operate at relatively low efficiencies, on the order of 25-50%, particularly at the moderate (2000 s) specific impulses of interest to many near-term missions.[4] This low thrust conversion efficiency results primarily from frozen flow losses and the large fraction of the input power that is dissipated as heat in the anode. For thrusters operating at power levels of one megawatt or lower, the anode power fraction can range from 50 up to 90%.[5] Although frozen flow losses can be minimized by using low-ionization energy materials such as Lithium, enabling an MPD thruster to provide the high-power, high-efficiency propulsion necessary for Exploration missions will require methods to significantly reduce the fraction of power wasted in the anode.

C. The Anode Fall and Onset Phenomena

Power is deposited, and thus wasted, in the anode by several mechanisms, including acceleration of electrons into the anode, plasma radiation, radiation from the hot cathode, and plasma flow energy convected to the anode. In most MPD thruster operating regimes, the dominant cause of the anode power fraction is the acceleration of electrons into the anode by the anode fall voltage.[6] When a voltage is applied between the electrodes and plasma begins to flow along the thruster, a large fraction of the total thruster voltage drop concentrates in a thin region near the anode, as shown in Figure 2.[7] This large voltage fall accelerates electrons towards the anode, and the energy they gain through this potential drop is lost as heat when they impact the anode. The anode fall is caused in part by depletion of charge carriers near the anode; this depletion is commonly called "anode starvation" and is associated with the "onset" of unstable current behavior, localized arcing, and anode erosion. A number of theories have been proposed to explain the anode starvation, anode fall, and onset behavior. The earliest theories modeled the anode fall as a simple sheath effect, and the onset phenomenon has been associated with conditions where the back-EMF due to plasma motion through the self-field exceeds the applied voltage.[8] More recent theories of the anode fall have included non-ideal effects, and the Hall effect has been identified as the primary cause.[3]

Without the Hall effect, the current in an MPD thruster would flow more or less radially from one electrode to the other (assuming, for the time being, that the thruster has the simple coaxial geometry shown in Figure 1). However, in MPD thrusters, the Hall effect causes the current to flow axially as well as radially. The generalized form of Ohm's law is given by

$$\mathbf{E} + \mathbf{V} \times \mathbf{B} = \frac{\mathbf{J}}{\sigma} + \frac{\left(\mathbf{J} \times \mathbf{B} - \nabla P_e\right)}{en_e}, \tag{1}$$

where σ is the plasma conductivity, n_e is the electron density, and P_e is the electron pressure. Since the anode material typically has a high conductivity, the axial electric field near the anode surface is negligible. With the further assumption that the axial derivative of the electron pressure can be neglected, the $\hat{z}$ component of Ohm's law gives the approximate magnitude of the axial current in self-field flow as

$$J_z \approx -\frac{\sigma B_\theta}{en_e} J_r = \Omega J_r, \tag{2}$$

where Ω is the electron Hall parameter. This axial current flowing across the azimuthal magnetic field causes a **J**x**B** force on the plasma in the negative radial direction, as shown in Figure 3, and this radial force pushes the plasma away from the anode, depleting the density near the anode. The decrease in density in turn increases the Hall effect,

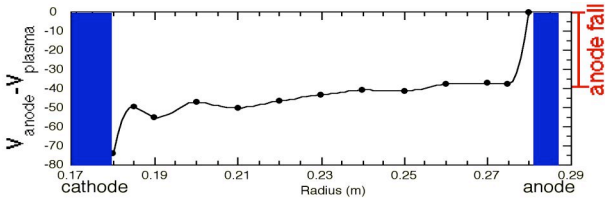

Figure 2. Example of an anode fall voltage measured in the CTX coaxial accelerator.[7]

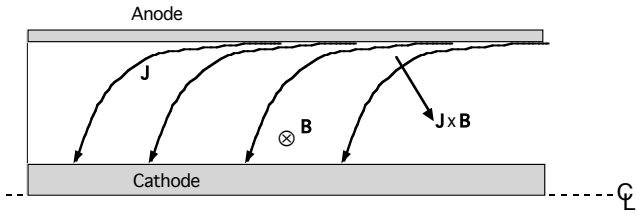

Figure 3. Conceptual illustration of current flow in an MPD thruster with the Hall Effect.

due to the inverse dependence of the axial current on the density expressed in Eqn. (2). This increases the axial current, further depleting the anode region… leading to a "vicious cycle". Thus the Hall effect feeds upon itself to reduce the plasma density near the anode until starvation and "onset" occurs. Once the anode region becomes starved, the Hall effect can cause large radial electric fields to develop near the anode through the action of the axial current flowing across the azimuthal field, as described by Ohm's law:

$$E_r \approx -\frac{1}{en_e}\left(J_z B_\theta + \frac{\partial P_e}{\partial r} \right). \tag{3}$$

Thus the Hall effect results in large voltage falls in the quasi-neutral plasma near the anode in addition to the space-charge potentials in the anode sheath caused by starvation. These large voltages and plasma starvation result in the "onset" phenomena, in which the thruster cannot deliver the current applied to it through steady-state processes and as a result, plasma instabilities and localized high-current arcs ("spot modes") deliver the electrons to the anode, resulting in power losses and damage to the electrode. Thus the Hall Effect results in large fractions of the power applied to a self-field MPD thruster to be wasted as heat in the anode.

Researchers at the Naval Postgraduate School have developed a nonlinear, ordinary differential equation that describes the entire plasma region affected by a planar anode, from the surface to the undisturbed plasma,[9] and have used numerical methods to solve this equation for a variety of plasma conditions.[10] Unfortunately for our application, their solution method presupposes knowledge of the anode fall magnitude and profile, and thus does not appear amenable to use in *predicting* anode fall voltages.

Experimenters at Princeton University have investigated the anode fall in MPD thrusters and found that the anode fall voltage in the spot mode is established by the minimum input power required to evaporate and ionize anode material so as to provide sufficient charge carriers in the anode region to support the applied thruster current.[11] Consequently, we hypothesize that if the effects of the Hall term can be counteracted to mitigate the anode plasma starvation, both the performance and lifetime of MPD thrusters can be improved significantly.

IV. Understanding the Hall Effect in MPD Thrusters Through Simulation

In order to develop a better understanding of the role the Hall Effect plays in the behavior and performance of MPD thrusters, we performed a number of simulations of a MPD thruster with and without the Hall effect term active in the simulation. For these simulations, we used the GRC Benchmark Thruster geometry, for which extensive data on thrust and voltage measurements are available.[12] The GRC Benchmark Thruster geometry is illustrated in Figure 4. In all of the simulations, the thruster was operated with a mass flow of 0.5 g/s of Argon propellant.

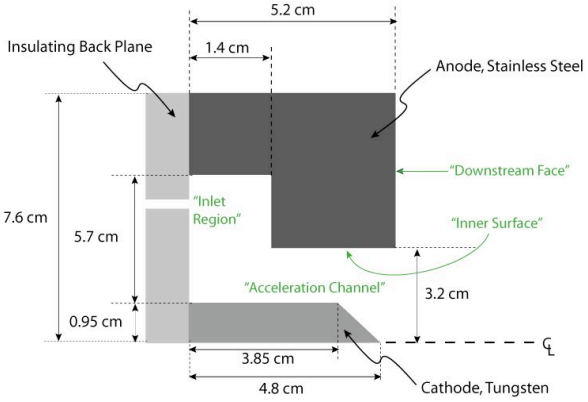

Figure 4. The GRC Benchmark Thruster geometry used in the simulations.

Current Flow and Plasma Flow

The impact of the Hall effect term in Ohm's law on the operation of the GRC thruster can be observed in a comparison among Figure 5 through Figure 8, which show the current flow lines and the plasma flow streamlines in simulations of the GRC Benchmark thruster at low (5kA) and high (15kA) current levels, with and without the Hall term. These simulations all used a mass flow rate of 0.5 g/s of Ar. At low current levels, there is little difference between the results obtained with and without the Hall Effect, as shown in Figure 5 and Figure 6. At these low current levels, the current density is relatively well distributed along the length of the acceleration chamber, and the current flows mainly radially between the electrodes. At the higher current level, which is just below the current level where experimentation has shown that the thruster operation becomes unstable,[13] the Hall Effect results in

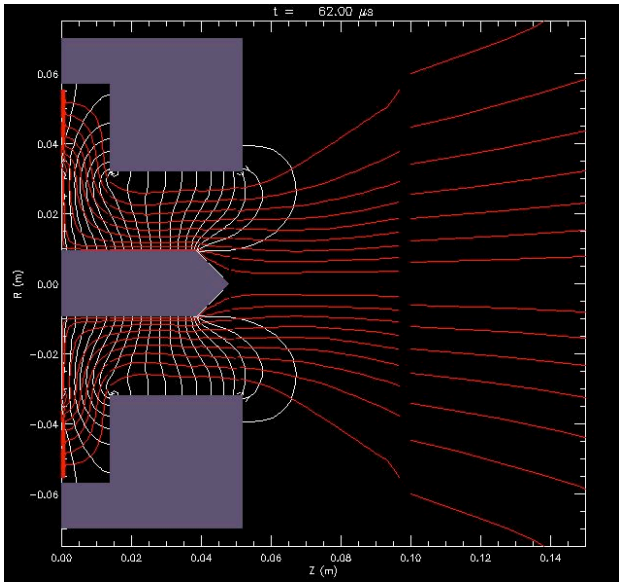

Figure 5. Current flow lines (white) and plasma flow streamlines (red) in the GRC thruster, without Hall Effect. (5 kA, 0.5 g/s)

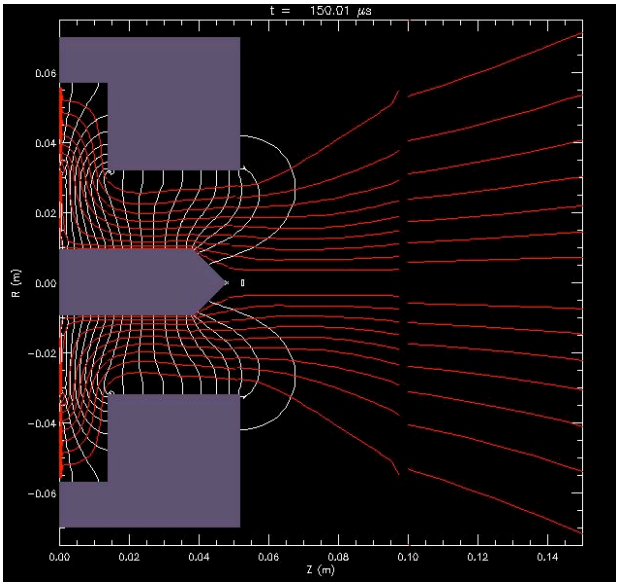

Figure 6. Current flow lines (white) and plasma flow streamlines (red) in the GRC thruster, with Hall Effect. (5 kA, 0.5 g/s)

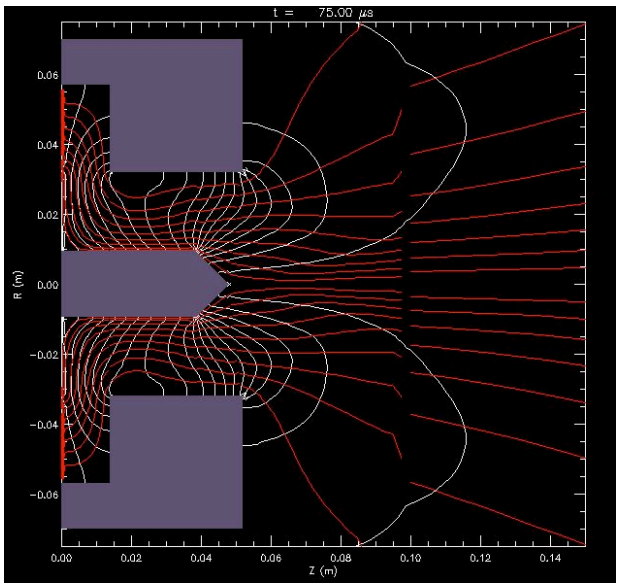

Figure 7. Current flow lines (white) and plasma flow streamlines (red) in the GRC thruster, without Hall Effect. (15 kA, 0.5 g/s)

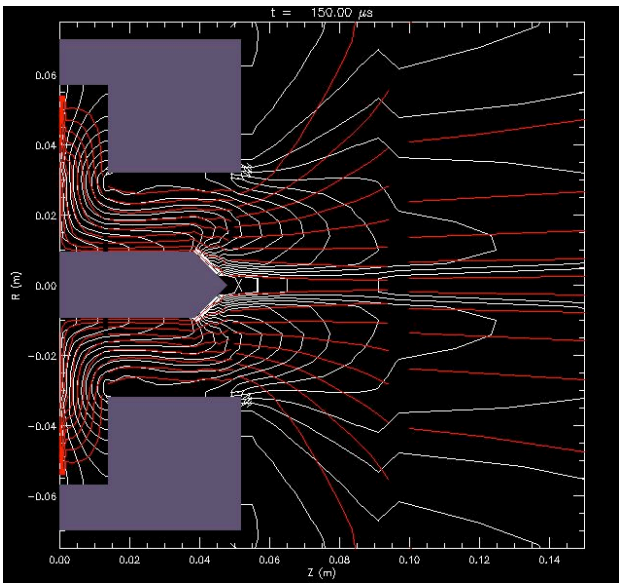

Figure 8. Current flow lines (white) and plasma flow streamlines (red) in the GRC thruster, with Hall Effect. (15 kA, 0.5 g/s)

significant distortion of the current flow paths, as can be seen in a comparison between Figure 7 and Figure 8. The simulation at high current without the Hall effect has current flow lines distributed relatively smoothly along the inner face of the anode. However, when the Hall Effect is taken into account, shown in Figure 8, the current in the cathode region becomes more concentrated at the cathode tip, and near the anode, the flow lines that attached to the inner face of the anode in Figure 7 are now forced downstream and attach primarily near the corner between the inner surface and downstream face of the anode. There is virtually no current flow to the inner cylindrical surface of the anode.

Plasma Density

Figure 9 through Figure 12 show plots of the electron density in the thruster in the same set of simulations. Again, at low current levels the Hall Effect term has little impact. At higher current levels, in the case with the Hall Effect (Figure 12), we see that the anode-region plasma near the exit corner, where the anode current is concentrated, is significantly less dense than in the case without Hall effect, and the Hall effect results in the plasma

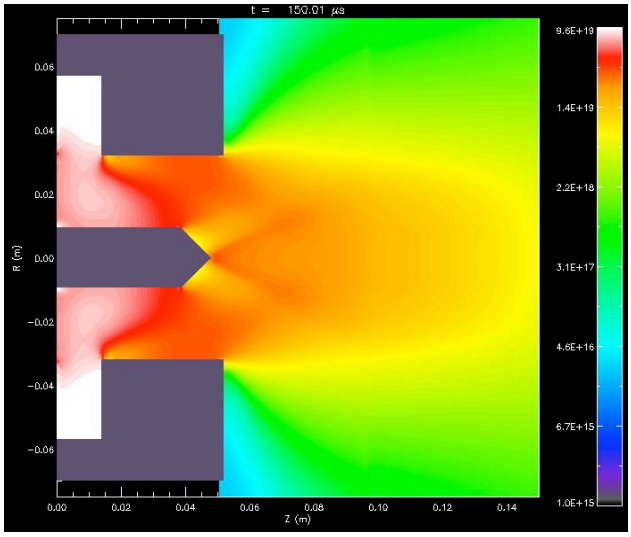

Figure 9. Electron density plot (m^{-3}), without Hall effect. (5 kA, 0.5 g/s)

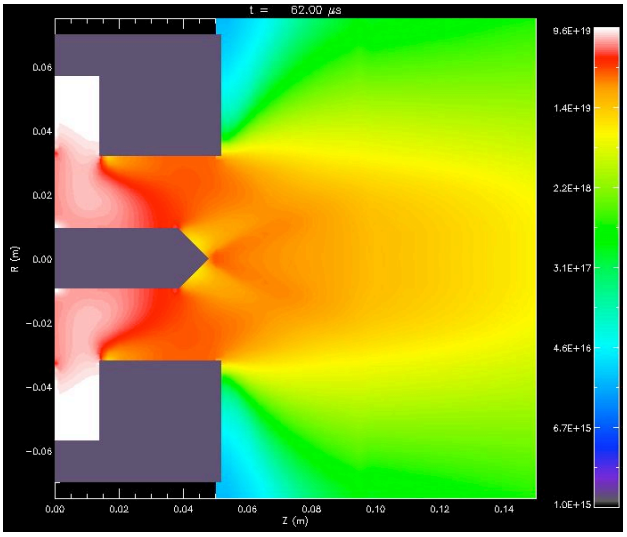

Figure 10. Electron density plot (m^{-3}), with Hall effect. (5 kA, 0.5 g/s)

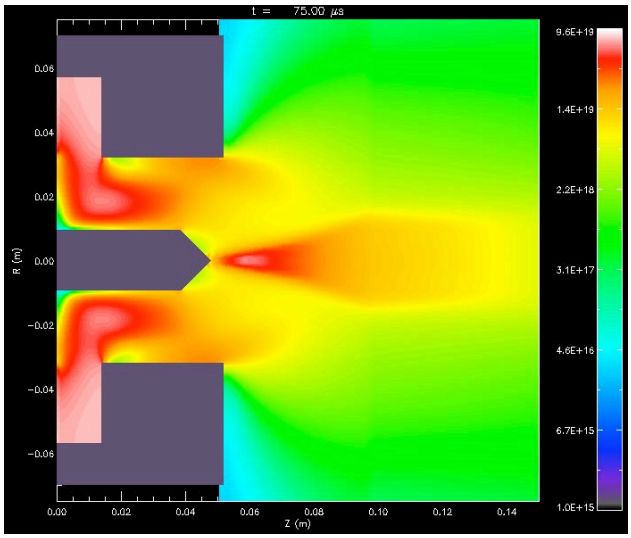

Figure 11. Electron density plot (m^{-3}), without Hall effect. (15 kA, 0.5 g/s)

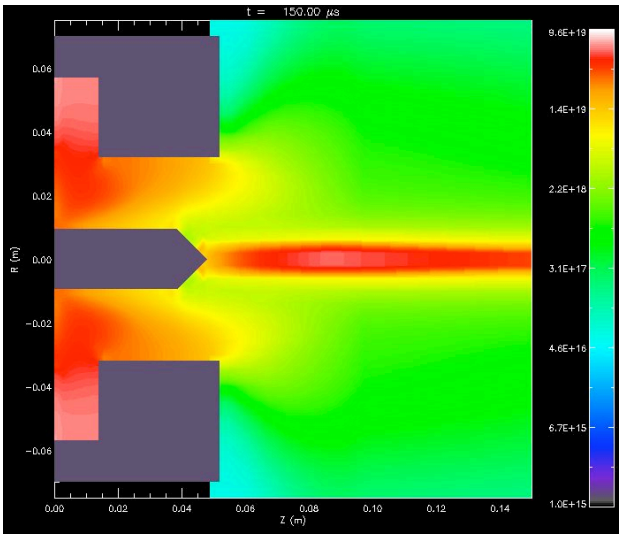

Figure 12. Electron density plot (m^{-3}), with Hall effect. (15 kA, 0.5 g/s)

being concentrated near the thruster axis. Without the Hall effect, the plasma near the inner surface of the anode, where most of the current lines attach in Figure 7, is at a density of roughly 5e19m^{-3}. With the Hall effect, however, the corner region where most of the current lines attach to the anode is at a much lower density of approximately 5e18 m^{-3}.

Critical Current Density

Although MACH2 cannot directly capture the physics of the anode fall and plasma sheath, we can obtain a measure for estimating when and where an anode fall and onset will occur by comparing the current density in the thruster to the electron thermal current in the anode region plasma. We can construct a simple 1-D model of the anode sheath by treating the anode as an infinite plate exposed to a plasma, and biased to a voltage V_A. The distribution function for the electrons and ions in a two-species Maxwellian plasma is

$$f_{e,i}\left(v_\perp, v_\parallel\right) = \frac{n_{e,i} m_{e,i}}{2\pi e T_{e,i}} \exp\left\{\frac{-m_{e,i}}{2eT_{e,i}}\left(v_\perp^2 + v_\parallel^2\right)\right\}. \tag{6}$$

The current density flowing to the surface of the conductor is obtained by integrating the unidirectionally accelerated or uniderectionally decelerated particle flux over all velocities directed towards the plate at the plate's surface:[14]

$$J_{e,i} = q_{e,i} \frac{n_{e,i} m_{e,i}}{2\pi e T_{e,i}} \int_{v_\perp = \sqrt{\max\left(0, \frac{-2q_{e,i}V_A}{m_{e,i}}\right)}}^{\infty} \int_{-\infty}^{+\infty} v_\perp \exp\left\{\frac{-m_{e,i}}{2eT_{e,i}}\left(\left(v_\perp^2 + \frac{-2q_{e,i}V_A}{m_{e,i}}\right) + v_\parallel^2\right)\right\} dv_\perp dv_\parallel. \tag{7}$$

$$J_{e,i} = q_{e,i} n_\infty \sqrt{\frac{eT_{e,i}}{2\pi m_{e,i}}} \begin{cases} 1 & q_{e,i}V_A \le 0 \\ e^{\left(\frac{-q_{e,i}V_A}{eT_{e,i}}\right)} & q_{e,i}V_A > 0 \end{cases}. \tag{8}$$

From (8), we see that the maximum electron current density that the sheath can transmit to the anode, barring nonideal effects, is the electron thermal current density at the sheath edge,

$$J_{e,th} = e n_e \sqrt{\frac{eT_e}{2\pi m_e}}. \tag{9}$$

For our simulation analyses here, we will define the "critical current density" as the ratio of the current to the electron thermal current

$$J_{crit} = J \Big/ J_{e,th}. \tag{10}$$

Although values of J_{crit} in excess of unity in the bulk plasma can be supported by a combination of electron and ion flow, when the simulations predict that J_{crit} is significantly larger than unity in the region adjacent to the anode surface, we can expect that a large anode fall must develop in order to cause additional charge carrier production through nonideal phenomena, such as electrode erosion or bulk plasma instabilities, in order to support the super-critical current levels.

Figure 13 through Figure 16 show plots of the current density divided by the electron thermal current for simulations with and without the Hall effect. The regions of white color are where $J/J_{e,th}$ exceeds unity. At low current levels, there is little difference between the cases with and without the Hall term. In the simulations at 15 kA, With the Hall effect, we see a larger region near the anode where the current density exceeds $J_{e,th}$, including the corner region where most of the current lines attach to the anode. Because the current densities exceed the thermal current in the regions near the anode and cathode where most of the current flows to the electrodes, we can expect that the plasma sheaths near these surfaces must develop large voltages in order to transport the electron current across the sheath.

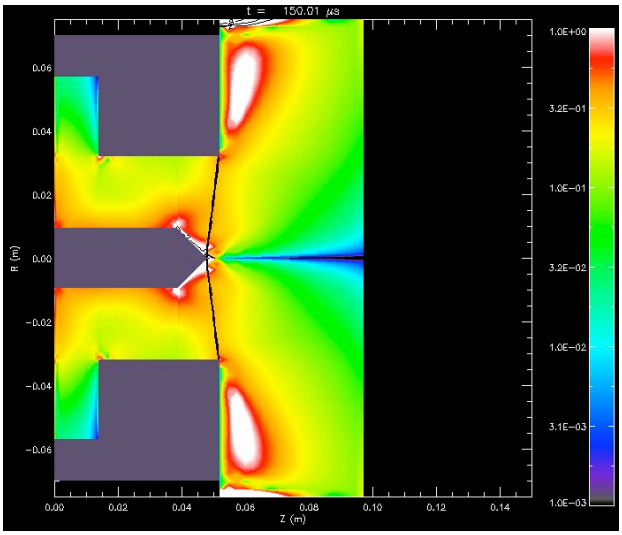

Figure 13. Plot of $J/J_{e,th}$, the current density normalized by the electron thermal current, without Hall effect.* (5 kA, 0.5 g/s)

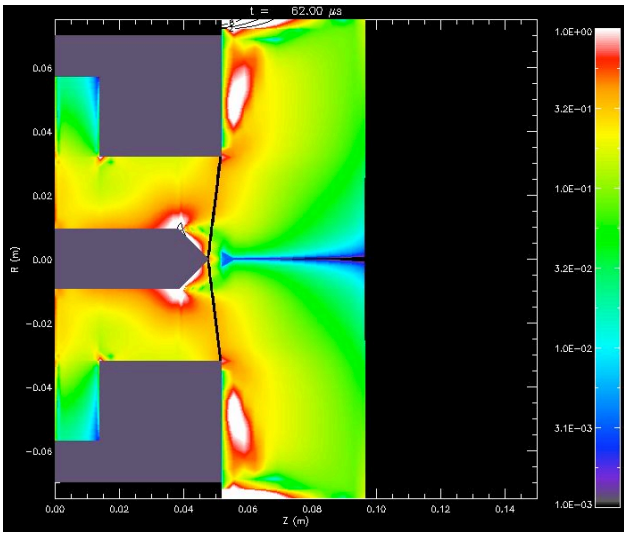

Figure 14. Plot of $J/J_{e,th}$, the current density normalized by the electron thermal current, with Hall effect. (5 kA, 0.5 g/s)

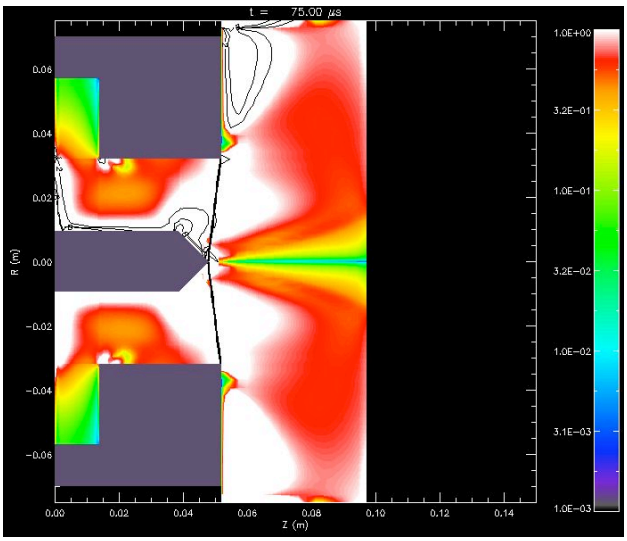

Figure 15. Plot of $J/J_{e,th}$, the current density normalized by the electron thermal current, without Hall effect. (15 kA, 0.5 g/s)

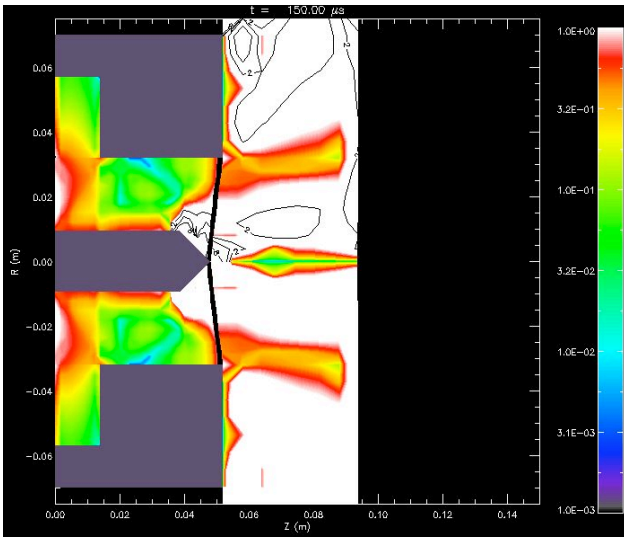

Figure 16. Plot of $J/J_{e,th}$, the current density normalized by the electron thermal current, with Hall effect. (15 kA, 0.5 g/s)

These results provide strong confirmation of the hypotheses that the action of the Hall effect results in depletion of the plasma electron densities in the region where the electrons flow to the anode surface as well as concentration of the current density near the anode lip. When $J/J_{e,th}$ exceeds unity near the anode surface the anode plasma sheath must develop a large voltage potential in order to support electron currents above $J_{e,th}$ into the anode.

* The black lines at the thruster exit and the discontinuities in the contours between the multiple blocks of the simulation are an artifact of the way in which the contours of J/J_{th} are calculated and plotted for a multiblock dataset.

V. Design and Simulation of Magnetic Nozzles for the GRC Benchmark Thruster

Our investigation of the effects of the Hall term on the operation of MPD thrusters has identified several guidelines for creating applied magnetic nozzles for these thrusters. Based on the results described above, an "optimum" magnetic nozzle must incorporate and balance the following aspects:

- **Moderate magnetic field perpendicular to anode surface:** In order to provide a $J_\theta B_r$ term in Ohm's law to counteract the $B_\theta J_r$ Hall term and enable electron current to flow radially to the anode with a low voltage drop, the magnetic nozzle should provide an applied field with magnetic field lines intersecting the anode surface. The applied field should be comparable to the self-field at the anode surface (B_{rz}~50-80% B_θ). This aspect can largely be optimized through vacuum-field calculations, but for full optimization we must use simulations to take into account the effects of plasma flows and currents on the magnetic field topology.
- **Achieve diffuse electron current profile on anode:** In order to minimize or eliminate the regions where the electron current at the anode exceeds the electron thermal current, the applied field should be designed to achieve a smooth distribution of the current along the acceleration channel. This aspect must be optimized primarily through iteration between design and simulation
- **Maximize plasma density at anode surface:** In addition to reducing peak current densities at the anode, the magnetic nozzle can also serve to increase plasma densities near the anode, thus increasing the electron thermal current to the anode. A magnetic nozzle can achieve this plasma density increase through several means: by guiding plasma flow to the anode along magnetic field lines; by inducing azimuthal rotation of the plasma which in turn causes centrifugal forces to push the plasma out towards the anode, and by altering current flow paths to achieve $J_{r,z} \times B_\theta$ forces which direct the plasma towards the anode.
- **Maximize concentration of plume flow in axial direction:** The magnetic nozzle will not improve the thruster's net performance if the field causes the plasma in the thruster plume to spread out at a large angle. Thus the field must be shaped to either force the flow towards the axis (through $J_{r,z} \times B_\theta$ effects), or to enable efficient detachment of the plasma from the field.
- **Minimize mass and power requirements for generating the magnetic field:** Because mass and power are always constrained quantities in space missions, the magnetic coil design must seek to minimize the mass, volume, and power consumption impacts for using the applied magnetic nozzle. A full optimization of the nozzle design thus must also account for requirements for structural support, thermal insulation and dissipation, as well as the complexity, mass, and cost of the power systems required to drive the coils.

Note that the last two guidelines are somewhat contradictory, in that we would like to push plasma out to the anode to maintain high density in that region while pushing plasma in to the axis to maximize net axial thrust. Consequently, the magnetic nozzle design must balance these aspects in order to optimize the net thrust.

Magnetic Nozzle Concepts

Based upon the guidelines above, we developed designs for several candidate magnetic nozzles. Figure 17 shows the vacuum field line configuration of a "traditional" solenoidal coil such as has been used in the past in applied-field testing of the GRC Benchmark thruster. Figure 18 shows the first new concept tested, labeled the "N1" nozzle, which uses two identical short coils, one located near the back plane of the thruster and the other near the exit plane of the thruster, biased with opposite polarities, to produce vacuum field lines that intersect the anode surface and diverge downstream of the thruster. Figure 19 shows the "N4" field configuration, which uses a conical coil positioned about 5 cm downstream of the thruster exit plane to achieve a more gentle divergence of the field. Figure 20 shows the "N5" configuration, where the conical coil is moved up to the thruster exit plane, and the currents in the coils are chosen so that the total net azimuthal coil current is zero.

A. Magnetic Nozzle Effects on GRC Benchmark MPD Thruster Performance

Using the modified MACH2 code, we simulated operation of the GRC Benchmark thruster at current levels ranging from 5 kA to 17.5 kA both in self-field operation and in applied field operation with a variety of magnetic nozzle geometries and strengths. All simulations were performed with a mass flow of 0.5 g/s of Argon.

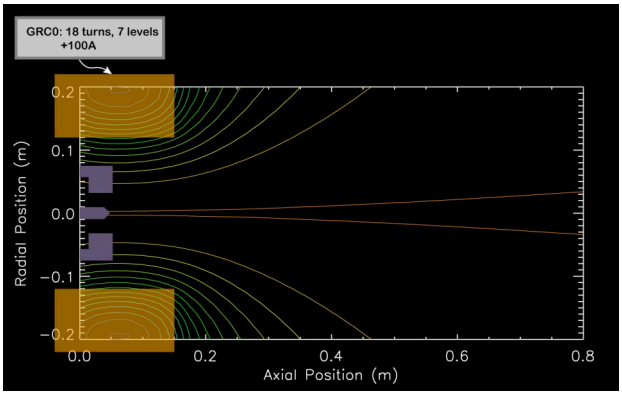

Figure 17. Field line plot of the "GRC0" conventional solenoid field for the GRC Benchmark geometry.

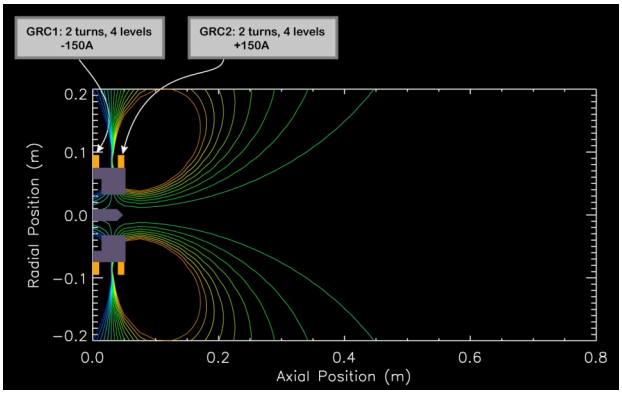

Figure 18. Field line plot of the "N1" Magnetic nozzle for the GRC Benchmark geometry.

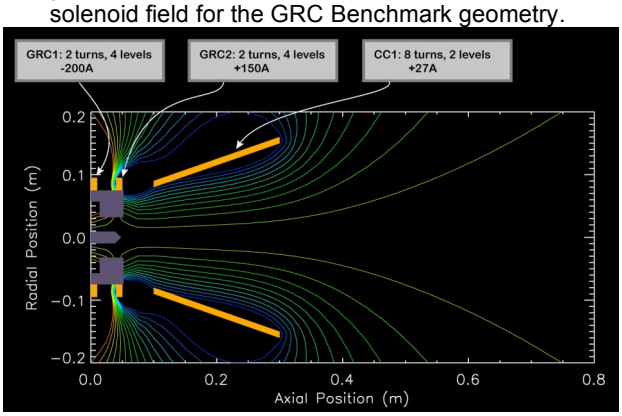

Figure 19. Field line plot of the "N4" Magnetic nozzle for the GRC Benchmark geometry.

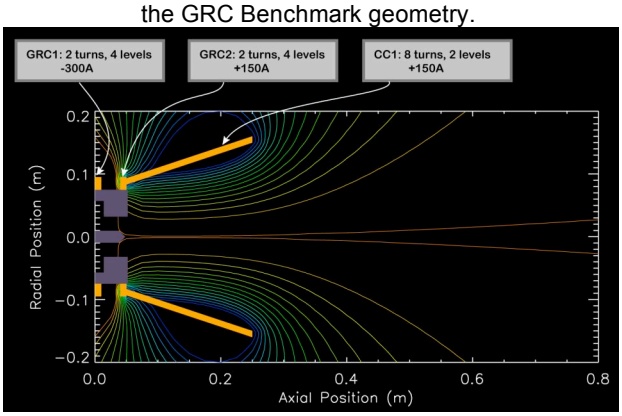

Figure 20. Field line plot of the "N5" Magnetic nozzle for the GRC Benchmark geometry.

Thrust and Voltage Characteristics

The net performance of the thruster predicted by the simulation in the various operating modes is summarized in the plot of thrust versus current in Figure 21 and the plot of voltage versus current in Figure 22. In these plots, the "N4x1" annotation indicates that the applied field used the N4 geometry, with -200 amps in Outer Coil 1, 150 amps in Outer Coil 2, and 28 amps in the Conical Coil. The annotation "N4x2" signifies that the same magnetic geometry was applied, but with twice the current levels in all the coils. For all of the curves shown in the figure, the points shown represent the current range over which a successful simulation was obtained. For example, with the N4 geometry, stable & convergent simulation results were obtained in the region of 5-10 kA with a "single-strength" field (N4x1), but above 10 kA the simulation would terminate due to a numerical or perhaps physical instability. If the strength of the field is doubled, however (N4x2), stable simulations were obtained only at higher current levels of 10-15 kA. Of particular importance to note is that the self-field simulations were successful only up to a current level of 12 kA. Above this current level, the simulation inevitably terminates due to instabilities that appear to be most severe in the anode region of the simulation. Two partially successful simulations were obtained in self-field operation at 15 kA, but the simulation still terminated before the flow field reached a true steady-state, and thrust level was much lower than at the moderate current levels.

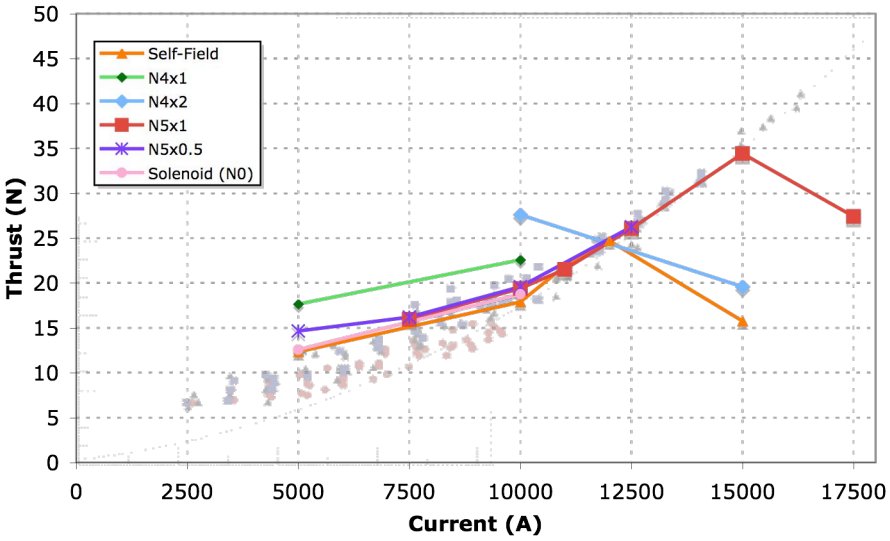

Figure 21. Variation of thrust with current for self-field operation and operation with several different magnetic nozzle geometries and strengths (mass flow = 0.5 g/s). Also shown (transparent red and blue points) are experimental thrust measurements from GRC/OAI testing of the benchmark thruster.

Figure 21 shows that, in general, the thrust levels predicted by the MACH2 code agree well with the experimental results obtained in self-field testing of the thruster by NASA/GRC/OAI researchers.[12] The simulations indicate that at the lower end of the current range, the magnetic nozzles can improve the thrust produced by the device by up to 43%. This improvement is obtained mainly because in low-current, self-field operation the thruster plume has a relatively large divergence, and the applied magnetic nozzle helps to focus the plume along the axis, resulting in more net axial thrust. At higher current levels (10-12 kA), the thrust is roughly the same for the self-field and the N5 applied field cases; this is likely due to the fact that the Hall Effect tends to focus the self-field plume along the axis at the higher current levels, so the magnetic nozzle provides little benefit in this respect.

At higher current levels, however, the magnetic nozzle appears to provide a significant benefit in that it enables stable operation of the thruster. Without the applied field, consistent stable simulations could be obtained up to only about 12 kA. With the N5 nozzle geometry, simulations were successful at up to 17.5 kA, and produced thrust levels significantly higher than the self-field case. Whether stable operation in simulation actually does translate to stable operation in real world use remains to be proven through experimental investigations.

The thruster voltages predicted by the MACH2 code, shown in Figure 22, are well below those observed in experimental testing of the benchmark thruster. This is not surprising, as the MACH2 code does not model the sheath voltages near the electrodes, and as discussed previously, the anode and cathode falls can represent a large fraction of the total thruster voltage. The simulations can be useful, however, for evaluating the effect of the applied magnetic nozzles on the component of the voltage due to bulk plasma physics. At low current levels, there is no significant difference between the self-field and applied field voltages. At higher current levels, the N5 geometry appears to be capable of lowering the thruster voltage by roughly 25% while maintaining or even increasing the thrust level. This voltage decrease is believed to be due to improvement in the uniformity of the current flow pattern, as will be described in the following subsection.

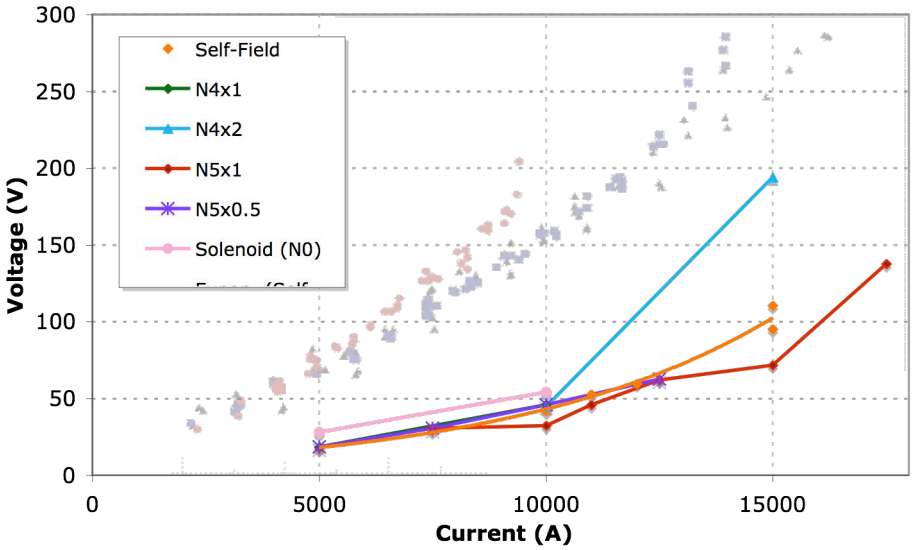

Figure 22. Variation of thruster voltage with current for self-field operation and operation with several different magnetic nozzle geometries and strengths (mass flow = 0.5 g/s). Also shown (red and blue points) are experimental data from GRC/OAI testing of the benchmark thruster.

Because the thruster voltage, and thus the input power, varies with the applied field configuration and current level, comparison of the predicted thrust performance of the thruster should account for the variations in input power. In Figure 23, we plot the "thrust efficiency multiplier" for the various cases, in which the thrust-to-voltage ratio is compared to the equivalent ratio in self-field operation:

$$M = \frac{\left(\text{Thrust with nozzle}\right)}{\left(\text{Voltage with nozzle}\right)} \Bigg/ \frac{\left(\text{Self-Field Thrust}\right)}{\left(\text{Self-Field Voltage}\right)} . \tag{17}$$

This plot indicates that the N4 and N5 magnetic nozzle geometries may provide improvements in thruster efficiency ranging from 49% at low power levels up to nearly 300% at higher power levels where onset behavior occurs in self-field operation. Again, it is important to note that because the MACH2 simulations do not capture the full physics of the electrode plasma sheaths and voltage, actual mileage will vary, and the relative improvement provided by the magnetic nozzles may be significantly higher or perhaps even lower. Nonetheless, from this analysis we conclude that the new magnetic nozzle designs have strong potential for achieving significant thrust efficiency improvements.

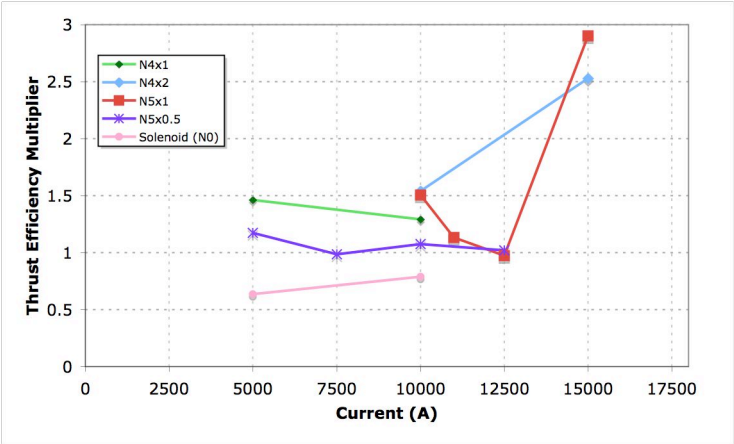

Figure 23. Predicted thrust efficiency multiplier for the various nozzle concepts.

Detailed Magnetic Nozzle Effects on Thruster Operation

The most significant effect of the applied magnetic nozzle is a dramatic improvement in the uniformity of the current distribution in the thruster and especially in the anode region. This effect is illustrated by a comparison between the plots of current flow in the self-field and applied field simulations in high-current operation in Figure 8 and Figure 24. In the 15 kA self-field case, the Hall Effect results in the anode current being concentrated in the inlet region, at the exit corner, and on the downstream face of the anode, with almost no current flowing to the anode along the inner cylindrical face. With the "N5" applied magnetic nozzle, however, the current flows mainly to the inner cylindrical face of the thruster, and is evenly distributed along that surface.

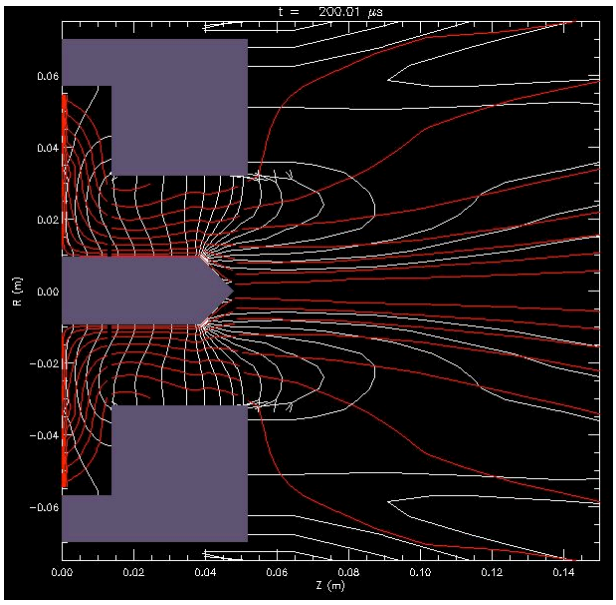

Figure 24. Current flow (white lines) and plasma flow streamlines (red lines) in the GRC Benchmark thruster with the "N5" Magnetic Nozzle. (15 kA, 0.5 g/s)

The electron density profiles in self-field and applied-field operation can be compared between Figure 12 and Figure 25. With the magnetic nozzle applied, the plasma density is much less concentrated on the axis; rather, the plume takes the form of a narrow annular cone. Another significant difference is that with the field applied, the region of high density at the inlet end of the thruster (the white and pink area) extends down to the beginning of the exit annulus, providing additional evidence that the acceleration of the plasma occurs primarily in the axial direction, as is desired.

Plots of the ratio of the current density to the electron thermal current are compared for self-field and applied-field simulations in Figure 16 and Figure 26. Although in the applied-field case there are still regions where the current density exceeds the thermal current at the anode, the important difference to note is that with the magnetic nozzle, the region where most of the current flows to the anode is below the critical current, except right at the exit corner of the anode. This result provides an encouraging indication that the magnetic nozzle will help to maintain adequate plasma density near the anode to prevent starvation and prevent formation of large anode falls.

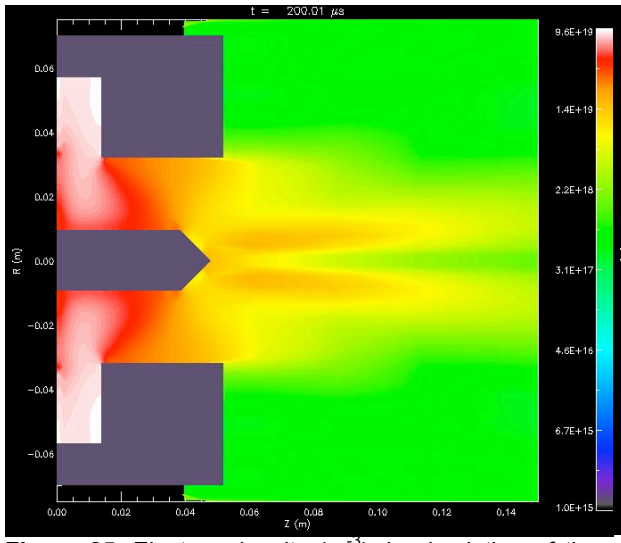

Figure 25. Electron density (m^{-3}), in simulation of the GRC Benchmark thruster with the "N5" Magnetic Nozzle. (15 kA, 0.5 g/s)

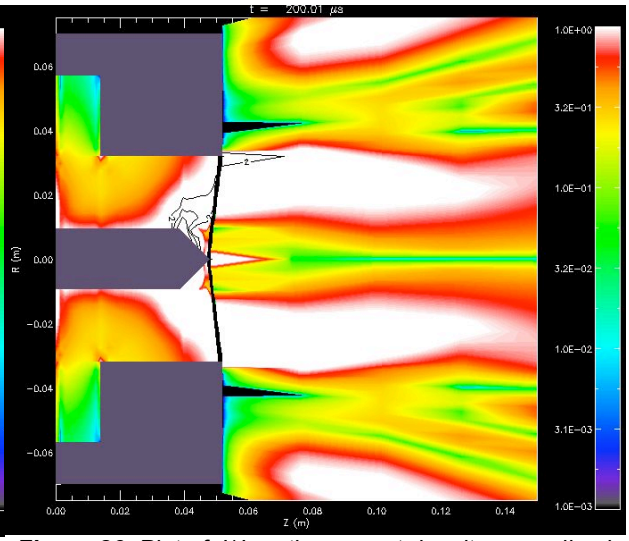

Figure 26. Plot of $J/J_{e,th}$, the current density normalized by the electron thermal current, in simulation of the GRC Benchmark thruster with the "N5" Magnetic Nozzle. (15 kA, 0.5 g/s)

VI. Conclusion

We have utilized numerical simulation tools to investigate the role the Hall Effect plays in the operation of MPD thrusters and to develop novel magnetic nozzle designs to counteract its negative effects and improve thruster performance. From comparisons of thruster simulations with and without the Hall term, we have found that the Hall Effect contributes to both reductions in plasma density and concentrations of current in regions near the anode surface. In operation at high current-to-mass-flow ratios, the plasma "starvation" and current concentrations result in the anode current density exceeding the current levels that the plasma can conduct to the anode through ideal, steady-state processes. To conduct the imposed current to the anode, a large voltage fall must develop near the anode to produce additional charge carriers through erosion of the anode and other non-ideal processes. To counteract this plasma starvation and current concentration, we have designed new applied magnetic nozzle configurations that provide moderate magnetic fields intersecting the anode surface and gently diverging magnetic fields downstream of the thruster. Simulations of the GRC Benchmark MPD thruster indicate that these magnetic nozzles can succeed in reducing anode current densities below critical levels. The simulation results also indicate that the magnetic nozzles can improve thruster efficiency by improving the extraction of axial thrust from the energy of the plasma emitted by the thruster.

VII. Acknowledgments

This work was funded by NASA/GRC Phase I SBIR contract NNC05CA62C. The author thanks S. Scott Frank, Jeffrey Slostad, and Sam Spitzer of TUI for their contributions to the mechanical design of the magnetic nozzle prototype. The author thanks Prof. Mitchell Walker of the Georgia Institute of Technology for his contributions to the project.

References

1. Meyers, R.M., Soulas, G.C., "Anode power deposition in applied-field MPD thrusters," AIAA Paper 92-6463,*28th JPC*, July 1992.
2. Soulas, G.C.,Meyers, R.M., "Mechanisms of anode power deposition in a low pressure free burning arc," AIAA paper IEPC-93-194.
3. Neiwood, E., *An Explanation For Anode Voltage Drops In An MPD Thruster*, Doctoral Thesis, MIT, April 1993.
4. Meyers, R.M., Soulas, G.C., "Anode power deposition in applied-field MPD thrusters," AIAA Paper 92-6463,*28th JPC*, July 1992.
5. Gallimore, A.D., Kelly, A.J., and Jahn, R.G., "Anode power deposition in quasi-steady MPD thrusters," AIAA Paper 90-2668, *21st IEPC*.
6. Soulas, G.C.,Meyers, R.M., "Mechanisms of anode power deposition in a low pressure free burning arc," AIAA paper IEPC-93-194.
7. Hoyt, R.P., *et al.,* "Magnetic Nozzle Design for Coaxial Plasma Accelerators," *IEEE Trans. Plas. Phys.* Vol. 23, No. 3, pp. 481-494, June 1995.
8. Miyasaka, T., Fujiwara, T., "Numerical Prediction of Onset Phenomenon in a 2-Dimensional Axisymmetric MPD Thruster," AIAA Paper 99-2432.
9. Biblarz, O., "Approximate Sheath Solutions for a Planar Plasma Anode," *IEEE Trans. Plas. Sci*., 19(6), Dec 1991, pp 1235-1243.
10. Biblarz, O., Brown, G.S., "Plasma-sheath approximate solutions for planar and cylindrical anodes and probes," *J. Appl. Phys.,* 73(12) 15 June 1993, pp 8111-8121.
11. Diamant, K.D., Choueiri, E.Y., Jahn, R.G., "Spot Mode Transition and the Anode Fall of Pulsed Magnetoplasmadynamic Thrusters," *J. Prop. & Power,* 14(6), p 1036-1042, Nov-Dec 1998.
12. Powerpoint slides titled "Magnetoplasmadynamic (MPD) Thruster: Baseline MPD Thruster Geometry", "Magnetoplasmadynamic (MPD) Thruster: Thrust Data, Various Mass Flow Rates (Ar)" and "Magnetoplasmadynamic (MPD) Thruster: Voltage Data, Various Mass Flow Rates (Ar)" provided by J. Gilland, NASA/GRC-OAI, personal commun,
13. "Magnetoplasmadynamic (MPD) Thruster Thrust Data, Various Mass Flow Rates", Glenn Research Center
14. Choinièri, E., *Theory And Experimental Evaluation of a Consistent Steady-State Kinetic Model For 2D Conductive Structures in Ionospheric Plasmas With Application To Bare Electrodynamic Tethers In Space*, Ph.D., Thesis, University of Michigan, 2004.